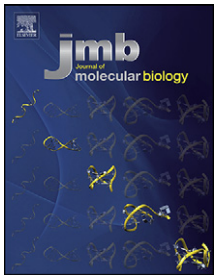

Dimer–Dimer Interaction of the Bacterial Selenocysteine Synthase SelA Promotes Functional Active-Site Formation and Catalytic Specificity

Yuzuru Itoh[1,2,3,†], **Markus J. Bröcker**[4,†], **Shun-ichi Sekine**[1,2,5], **Dieter Söll**[4,6] and **Shigeyuki Yokoyama**[1,2,7]

*1 - **Department of Biophysics and Biochemistry,** Graduate School of Science, The University of Tokyo, 7-3-1 Hongo, Bunkyo-ku, Tokyo 113-0033, Japan*
*2 - **RIKEN Systems and Structural Biology Center,** 1-7-22 Suehiro-cho, Tsurumi, Yokohama 230-0045, Japan*
*3 - **Laboratory of Membrane and Cytoskeleton Dynamics,** Institute of Molecular and Cellular Biosciences, The University of Tokyo, 1-1-1 Yayoi, Bunkyo-ku, Tokyo 113-0032, Japan*
*4 - **Department of Molecular Biophysics and Biochemistry,** Yale University, New Haven, CT 06520-8114, USA*
*5 - **Division of Structural and Synthetic Biology,** RIKEN Center for Life Science Technologies, 1-7-22 Suehiro-cho, Tsurumi, Yokohama 230-0045, Japan*
*6 - **Department of Chemistry,** Yale University, New Haven, CT 06520-8114, USA*
*7 - **RIKEN Structural Biology Laboratory,** 1-7-22 Suehiro-cho, Tsurumi, Yokohama 230-0045, Japan*

***Correspondence to Dieter Söll and Shigeyuki Yokoyama:** D. Söll is to be contacted at: Department of Molecular Biophysics and Biochemistry, Yale University, New Haven, CT 06520-8114, USA; S. Yokoyama, RIKEN Structural Biology Laboratory, 1-7-22 Suehiro, Tsurumi, Yokohama 230-0045, Japan. yokoyama@riken.jp*
http://dx.doi.org/10.1016/j.jmb.2014.01.003
Edited by M. Guss

Abstract

The 21st amino acid, selenocysteine (Sec), is incorporated translationally into proteins and is synthesized on its specific tRNA ($tRNA^{Sec}$). In Bacteria, the selenocysteine synthase SelA converts Ser-$tRNA^{Sec}$, formed by seryl-tRNA synthetase, to Sec-$tRNA^{Sec}$. SelA, a member of the fold-type-I pyridoxal 5′-phosphate-dependent enzyme superfamily, has an exceptional homodecameric quaternary structure with a molecular mass of about 500 kDa. Our previously determined crystal structures of *Aquifex aeolicus* SelA complexed with $tRNA^{Sec}$ revealed that the ring-shaped decamer is composed of pentamerized SelA dimers, with two SelA dimers arranged to collaboratively interact with one Ser-$tRNA^{Sec}$. The SelA catalytic site is close to the dimer–dimer interface, but the significance of the dimer pentamerization in the catalytic site formation remained elusive. In the present study, we examined the quaternary interactions and demonstrated their importance for SelA activity by systematic mutagenesis. Furthermore, we determined the crystal structures of "dependentamerized" SelA variants with mutations at the dimer–dimer interface that prevent pentamerization. These dimeric SelA variants formed a distorted and inactivated catalytic site and confirmed that the pentamer interactions are essential for productive catalytic site formation. Intriguingly, the conformation of the non-functional active site of dimeric SelA shares structural features with other fold-type-I pyridoxal 5′-phosphate-dependent enzymes with native dimer or tetramer (dimer-of-dimers) quaternary structures.

Introduction

Selenocysteine (Sec) is known as the 21st amino acid incorporated translationally into proteins and is synthesized on its specific tRNA ($tRNA^{Sec}$) [1]. The $tRNA^{Sec}$-ligated serine (Ser-$tRNA^{Sec}$) generated by seryl-tRNA synthetase is converted to $tRNA^{Sec}$-ligated Sec (Sec-$tRNA^{Sec}$), where selenophosphate, synthesized by selenophosphate synthetase, is used as a selenium donor [2]. In Eukaryotes and

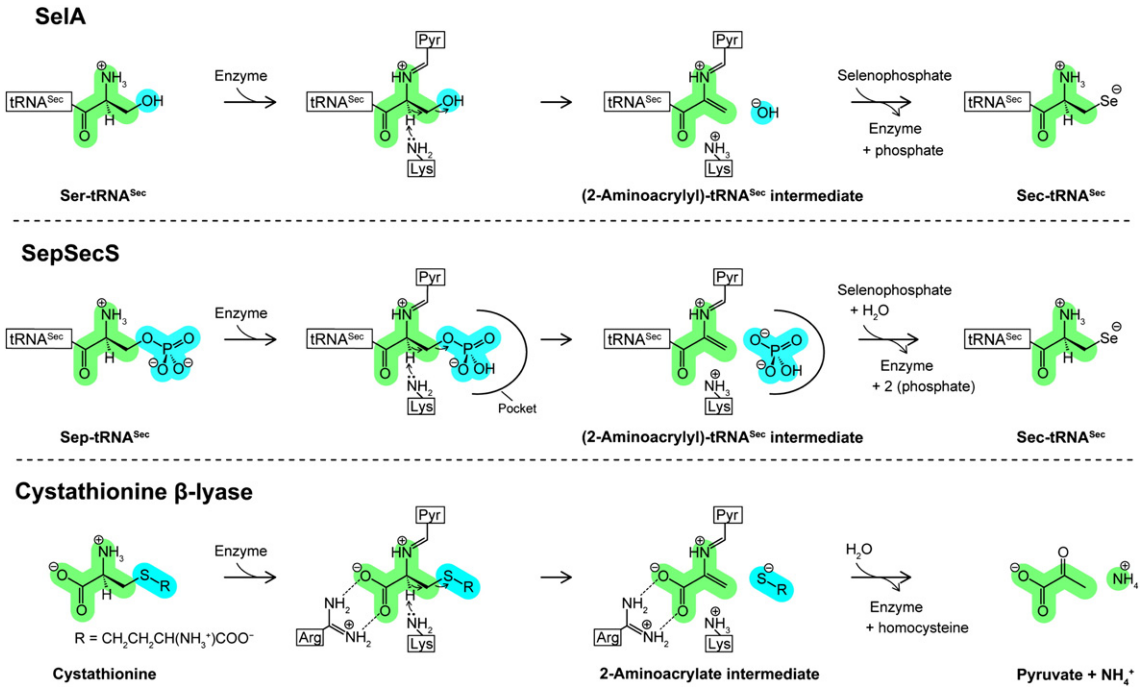

Fig. 1. The enzymatic reaction. Schematic views of the enzymatic reactions of SelA, SepSecS, and cystathionine β-lyase (CBL). These enzymes catalyze α position deprotonation, followed by β position elimination, to generate tRNA-ligated or non-esterified 2-aminoacrylate intermediates, conjugated with PLP. The substrate of CBL is cystathionine, and the enzyme–substrate interaction is responsible for the α-carboxyl group [8] (c) while SepSecS interacts with the phosphate group of its substrate Sep-tRNA^{Sec} [9]. However, Ser-tRNA^{Sec}, the substrate of SelA, has neither a carboxyl nor a phosphate group. Furthermore, the leaving group in the SelA-catalyzed reaction is a hydroxide ion, which is less suitable as compared to the phosphate and the deprotonated homocysteine eliminated in the SepSecS- and CBL-catalyzed reactions, respectively.

Archaea, Ser-tRNA^{Sec} is phosphorylated by *O*-phosphoseryl-tRNA^{Sec} kinase (PSTK) to generate *O*-phosphoseryl-tRNA^{Sec} (Sep-tRNA^{Sec}) [3], followed by Sep-to-Sec conversion catalyzed by SepSecS [4,5]. On the other hand, in Bacteria, the selenocysteine synthase SelA directly converts Ser-tRNA^{Sec} to Sec-tRNA^{Sec}, without a previous phosphorylation step [6]. Both SelA and SepSecS are pyridoxal 5′-phosphate (PLP)-dependent enzymes.

SelA is a homodecameric enzyme with an overall molecular mass of about 500 kDa. We previously determined the crystal structures of SelA with and without tRNA^{Sec} [7]. The SelA decamer is organized as a pentamer of intimate dimers, and it binds 10 tRNA^{Sec} molecules. Residues from each of the four SelA subunits of two intimate dimers are involved in processing one Ser-tRNA^{Sec} molecule, indicating that the decameric quaternary structure is essential to bind Ser-tRNA^{Sec} [7]. We proposed the SelA catalytic mechanism based on the co-crystal structure with thiosulfate, an analog of selenophosphate. While the tRNA-binding pocket is formed at the dimer–dimer interface, the significance of the formation of an $(\alpha_2)_5$ SelA structure in the generation of functional catalytic sites remained unclear.

The enzymes SelA and SepSecS belong to the largest PLP-dependent enzyme group, the fold-type-I superfamily, and catalyze the replacement of the amino acid β position (β replacement) in an α,β elimination reaction proceeding via a 2-aminoacrylate intermediate and a subsequent addition step (Fig. 1) [6]. Although β replacement is a common reaction, there are two major difficulties with the Sec synthesis step. First, the precursor, Ser-tRNA^{Sec}, lacks the α-carboxyl group, which is used for the substrate–enzyme interaction in all fold-type-I PLP-dependent enzymes that work with α-amino acids [10]. Second, the leaving group in the β elimination step is a hydroxide ion from the Ser moiety (Fig. 1) [6]. In general, a hydroxide ion is not a suitable leaving group, and no other fold-type-I members can eliminate it from the β position of an α-amino acid. In Eukarya/Archaea, these difficulties are overcome with the assistance of PSTK. PSTK phosphorylates the Ser moiety to generate Sep-tRNA^{Sec} [3], which is the

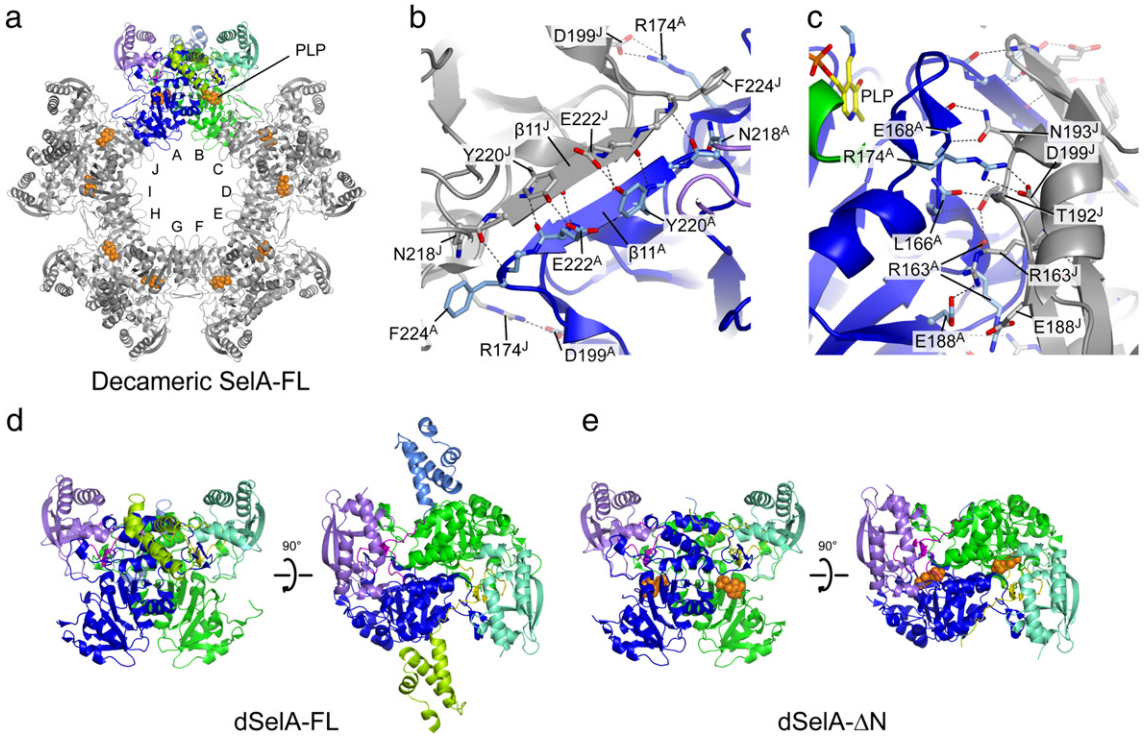

Fig. 2. Structure of SelA. (a) Overall view of the crystal structure of decameric SelA-FL. PLPs are represented as sphere models. The N-terminal domain, the N-linker, the core domain, and the C-terminal domain of subunit A are colored cornflower blue, magenta, blue, and medium-purple, respectively, while those of subunit B are colored green-yellow, yellow, green, and aquamarine, respectively. Subunits C–J are colored gray. (b and c) Close-up views of the interactions at interfaces I (b) and II (c) between intimate dimers. Interactions between subunits A and J are shown. The colors of the ribbon diagrams are the same as in (a). (d and e) Overall views of the dimeric SelA mutants, dSelA-FL (d) and dSelA-ΔN (e). The ribbon diagrams are colored as in (a). dSelA-FL lacks PLP.

substrate of SepSecS (Fig. 1). The β elimination is thus facilitated because the phosphate is an excellent leaving group. Furthermore, the phosphate group is predominantly responsible for the substrate binding to SepSecS [9]. In contrast, the bacterial system differs strikingly in that the single enzyme SelA directly

Table 1. *In vivo* mutational analyses of *E. coli* SelA

SelA mutant	Amino acid change *E. coli* numbering	*A. aeolicus* Numbering	Function of residue	PLP occupancy (Mut10a– Mut10d) (%)	Activity *in vivo*
1	ΔGln233–Thr236	Glu222–Val225	Decamerization interface I		–
2	ΔGln233–Gly234	Glu222, Gly223	Decamerization interface I		–
3	Arg185Ala	Arg174	Decamerization interface II/III		+++
4	Thr202Tyr	Thr191	Decamerization interface II/III		–
5	Thr203Tyr	Thr192	Decamerization interface II/III		–
6	His207Ala	Lys196	Decamerization interface II/III		+++
7a	Asp210Ala	Asp199	Decamerization interface II/III		+++
7b	Asp210Arg	Asp199	Decamerization interface II/III		–
8	ΔThr203–Asn204	Thr192, Asn193	Decamerization interface II/III		–
9	Thr202–Arg205 = 2 × Ala	Thr191–Lys194	Decamerization interface II/III		–
10a	Lys295Ala	Lys285	Covalent PLP ligand	n.d.	–
10b	Lys295Ala, Asp294Lys	Lys285, Asp284	Covalent PLP ligand	25	–
10c	Lys295Ala, Leu296Lys	Lys285, Leu286	Covalent PLP ligand	37	–
10d	Lys295Ala, Leu297Lys	Lys285, Leu287	covalent PLP ligand	30	–

+++, fully active; +, significantly reduced activity; –, inactive; n.d., below detection limit.
Mutations introduced in *E. coli* SelA, numbering of the corresponding residues for *A. aeolicus* SelA, and functions of the residues as determined from the structures and catalytic activities of the corresponding *E. coli* SelA variants *in vivo* are indicated. PLP occupancy for SelA variants 10a–10d is indicated. All SelA variants lacking catalytic activity *in vivo* were purified and tested for solubility to exclude the possibility that the activity loss was due to inclusion body formation.

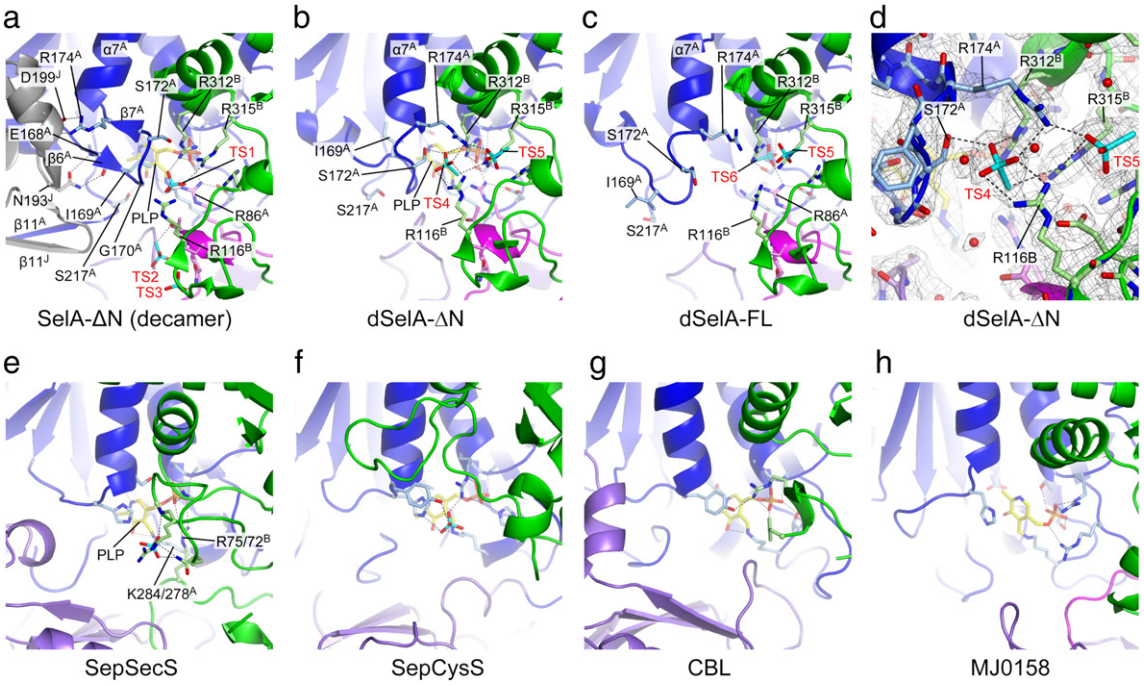

Fig. 3. Catalytic site comparison. (a–c) Catalytic site comparison between the decameric and dimeric SelAs. The β-sheet β6•β7 and α7 in the catalytic site also participate in the pentamerizing interaction in the decameric SelA-ΔN (a). On the other hand, dSelA-FL (b) and dSelA-ΔN (c) lack the β6•β7 sheet, and α7 changes its orientation; therefore, the catalytic site structure is disrupted. dSelA-FL also lacks PLP. Thiosulfate ions are bound in different sites among (a)–(c). Possible hydrogen bonds or ionic interactions are shown as broken lines. (d) Close-up view of the TS4- and TS5-binding sites of dSelA-ΔN. The $2F_o - F_c$ electron density map at the 1.0 σ level is shown. (e–h) Catalytic sites of SepSecS (PDB ID: 2Z67 [11]) (e), SepCysS (PDB ID: 2E7J [12]) (f), CBL (PDB ID: 1CL1 [12]) (g), and MJ0158 (PDB ID: 2AEV [13]) (h). They lack the β6•β7 counterpart, and the orientations of their α7 counterparts are closer to those of α7 in depentamerized SelA mutants. The phosphate/sulfate ions at the catalytic site are shown. The SepSecS structure 2Z67 is from the archaeon *Methanococcus maripaludis*. The focused Arg and Lys residues are labeled according to their numbering in human/*M. maripaludis* SepSecS.

converts Ser-tRNA^{Sec} to Sec-tRNA^{Sec}, without phosphorylation. Our previous study suggested a putative binding site for the 3′-terminal A76 of tRNA^{Sec}, and the binding site could compensate for the lack of the α-carboxyl group [7]. However, the mechanism that facilitates the hydroxyl-group elimination has not been elucidated.

In this study, we have determined the structural basis for productive SelA active-site formation, which requires the cyclization of SelA dimers to a full decamer. Analyses of the structures of *Aquifex aeolicus* SelA and dimeric SelA variants revealed that the active-site conformations of SelA intimate dimers differ significantly from those of decameric SelA. Structural rearrangements upon decamerization generate 10 catalytically functional active sites that properly accommodate and position Ser-tRNA^{Sec} for Sec formation. Based on a comparison of SelA with phylogenetically related enzymes, we describe a refined mechanism for the direct hydroxyl-group elimination facilitated by SelA and propose an evolutionary hypothesis for the emergence of the decameric SelA architecture.

Results and Discussion

The dimer–dimer interface in the pentamer-of-dimers structure of SelA

A. aeolicus SelA is a homodecamer in which the 10 subunits, designated here as subunits A to J, form a “pentamer of dimers” (Fig. 2a). The “intimate dimers” A•B to I•J have the largest intersubunit interfaces (e.g., A•B interface, 4067 Å^2) on which the enzyme active sites are built. Therefore, the intimate dimer is the basal building block of SelA. In the pentamer-of-dimers quaternary structure, intimate dimers I•J and A•B, for example, interact with each other through subunits J and A. The dimer–dimer interface encompasses 1140 Å^2 and characteristically constitutes the overall decameric arrangement of SelA. The dimer–dimer interface may be divided into three parts. The first part (part I, 438 Å^2) has internal 2-fold symmetry and is composed of two sets of residues from Asn218 to Phe224, constituting strand β11 within the core domain (Fig. 2b). Strand

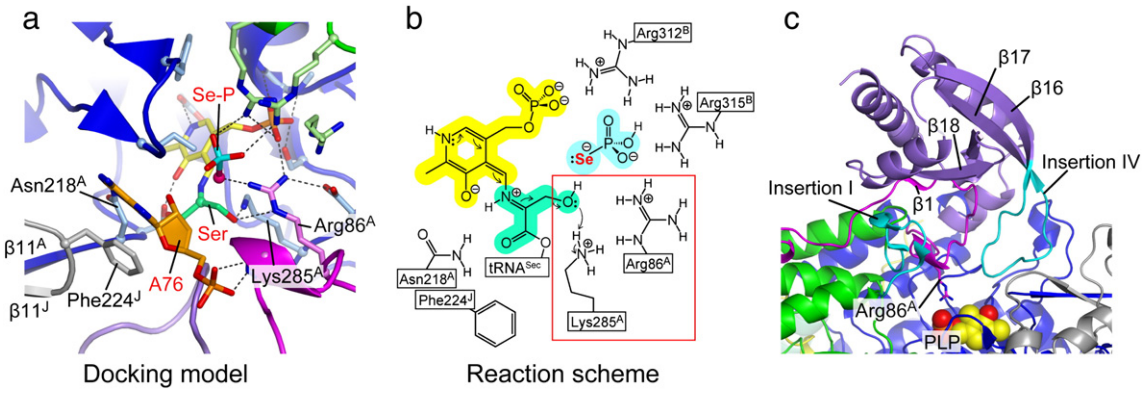

Fig. 4. Proposed scheme of the SelA-catalyzed reaction. (a) Docking model of the Ser-ligated terminal nucleotide (A76) of $tRNA^{Sec}$ and selenophosphate (Se-P). A76 and the Ser moiety are modeled based on the mutational analyses, and their carbon atoms are colored salmon and spring green, respectively. Arg86 is located in the vicinity of Lys285 and Ser. Phe224 from subunit J and Asn218 from subunit A form the A76-binding pocket. The Ser moiety is attached covalently to PLP. Se-P occupies the TS1-binding site. (b) The reaction scheme of the protonation of the β-hydroxyl group by Lys285, which enables the elimination of the leaving group (a water molecule). Arg86 may provide the basic environment to strengthen the Lys285 protonation activity. (c) The interaction interface between the core and C-terminal domains of SelA. The N-linker (magenta) and the SelA-specific insertions I and IV (cyan) participate in the interaction between the core and C-terminal domains. The other regions are colored as in Fig. 2a. β1 in the N-linker forms a β-sheet with β18 in the C-terminal domain. Arg86 in the N-linker participates in the catalytic site.

β11 from subunit J, for example, and the corresponding strand from subunit A form an antiparallel β-sheet between intimate dimers I•J and A•B. The other parts, II and III (307 $Å^2$ each), are symmetrically related to each other. Parts II/III between subunits J and A comprise Arg163, Leu166, Glu168, and Arg174 (η4-loop-β6-loop-β7) from subunit J and Glu188, Thr191, Thr192, Asn193, Lys196, and Asp199 (β8-loop-β9-α8) from subunit A and *vice versa* (Fig. 2c).

We introduced mutations into the dimer–dimer interface by using *Escherichia coli* SelA (Table 1). The amino acid residues in the dimer–dimer interface are conserved between the *A. aeolicus* and *E. coli* SelAs, although the conservation in part I is relatively low (Table 1). The Mut1 and Mut2 mutations were designed to impair the antiparallel β11•β11 interaction in part I, by deleting residues 222–225 and 222–223, respectively (residue numbering according to *A. aeolicus* SelA). The enzymes bearing the Mut1 and Mut2 mutations were catalytically inactive *in vivo* (Table 1), indicating that the integrity of strand β11 and the formation of the resultant antiparallel β-sheet are critical for the function of SelA. Mutations targeting parts II/III were also examined (Table 1). Here, the Ala mutations of individual residues in parts II/III exhibited no significant effects on the SelA activity (Mut3, Mut6, and Mut7a). In contrast, the Thr191Tyr, Thr192Tyr, and Asp199Arg mutations (Mut4, Mut5, and Mut7b), which were designed to cause steric clashes, inactivated *E. coli* SelA *in vivo*. Similarly, the deletion of Thr192–Asn193 (Mut8) or the replacement of four residues, Thr191–Lys194, with two Ala residues (Mut9) rendered *E. coli* SelA inactive *in vivo*. These results suggested that the integrity of parts II/III is also important for the SelA activity.

Crystal structure of dimeric SelA

The interface between the intimate dimers is much smaller than that between the subunits within the intimate dimer, suggesting weaker interactions between the dimer units. In fact, a quadruple mutation (Tyr220Pro-Asp199Arg-Thr191Tyr-Thr192Tyr) abolished the pentamerization and resulted in an inactive "dimerized" or "depentamerized" enzyme [7]. (In the following, we refer to the depentamerized enzyme as dimeric SelA.) Importantly, dimeric SelA is stable and can be purified for crystallization. In this study, we crystallized the full-length and N-terminally truncated (ΔN, deletion of residues 1–61) dimeric SelA proteins and determined their structures at 3.35 and 2.40 Å resolutions, respectively (Fig. 2d and e). The lysine residues of the dimeric full-length SelA (dSelA-FL) were methylated for crystallization improvement, while the dimeric SelA-ΔN (dSelA-ΔN) was crystallized without Lys methylation. The overall structures of dSelA-FL and dSelA-ΔN are similar to each other and to those of the intimate dimers of decameric SelA-FL and SelA-ΔN, respectively. Each subunit of dSelA-FL consists of the N-terminal domain (residues 1–66), the N-linker (residues 67–89), the

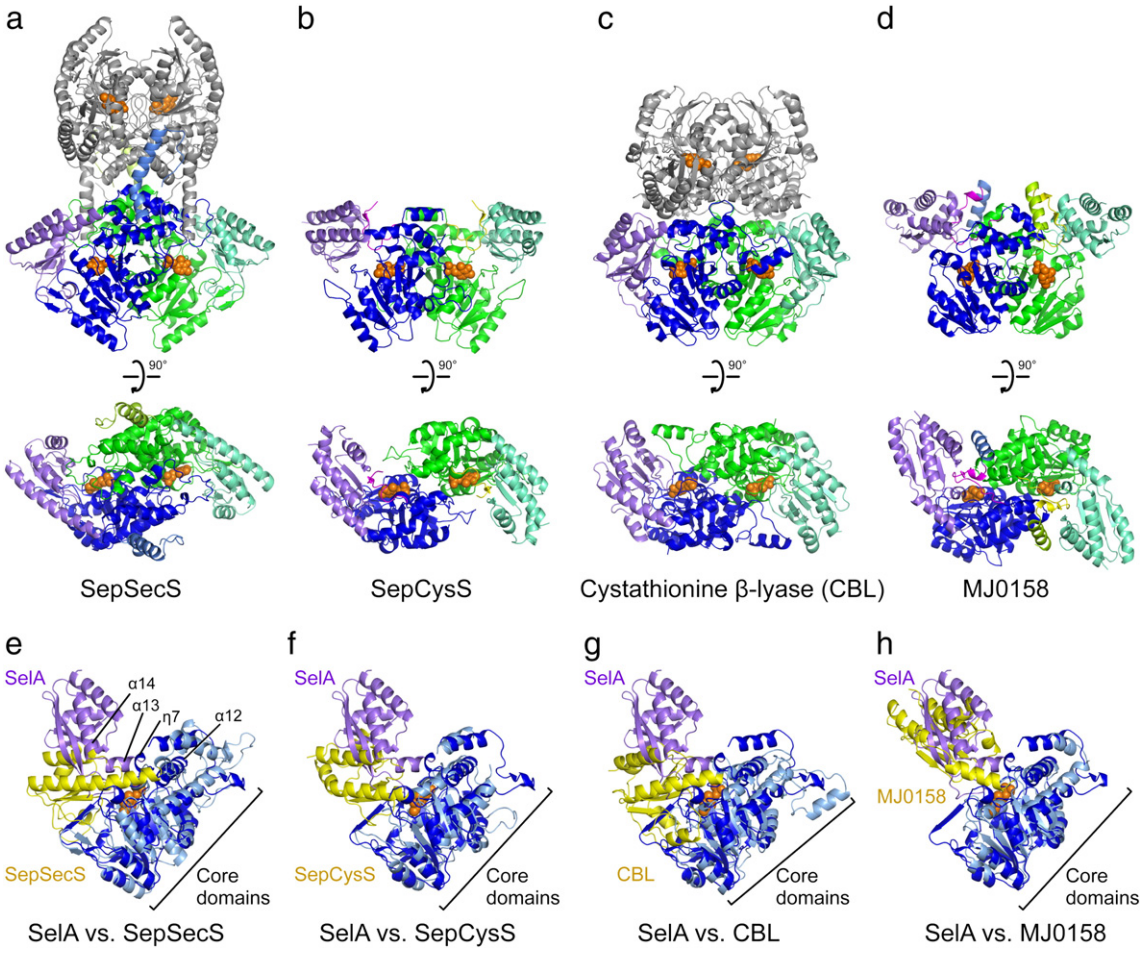

Fig. 5. Structure comparison with other fold-type-I PLP-dependent enzymes. (a–d) Overall crystal structures of SepSecS (PDB ID: 2Z67 [8]) (a), SepCysS (PDB ID: 2E7J [11]) (b), cystathionine β-lyase (CBL) (PDB ID: 1CL1 [12]) (c), and MJ0158 (PDB ID: 2AEV [13]) (d). The N-terminal domains, the N-linkers, the core domains, and the C-terminal domains of subunits A and B are colored as in Fig. 2a. The N-terminal regions of SepCysS and MJ0158 correspond to the SelA N-linker. Like the SelA N-linker, these regions form β-sheets with their C-terminal domains. On the other hand, the N regions of the homotetrameric enzymes SepSecS and CBL participate in the interactions between the two intimate dimers, and thus, they occupy different positions from that of the SelA N-linker. The intimate dimers C•D of SepSecS and CBL are colored gray in the top panels and are not shown in the bottom panels. (e–h) Comparison of the C-terminal domain orientation with SelA. The A subunits of SepSecS (e), SepCysS (f), CBL (g), and MJ0158 (h) were superposed on the SelA subunit A, by fitting their core domains. The core and C-terminal domains of SelA are colored blue and medium-purple, respectively, as in Fig. 2a, while those of the other PLP-dependent enzymes are colored light blue and yellow, respectively. The major helices α12 and α14, located in the core and C-terminal domains, respectively, are connected by the short helices η7 and α13 in SelA. In contrast, the α12 and α14 counterparts are directly connected in SepSecS and form a continuous single helix in SepCysS and CBL. On the other hand, MJ0158 has the α13 counterparts, and the orientation of its C-terminal domain is somewhat closer to that of the SelA C-terminal domain.

core domain (residues 90–338), and the C-terminal domain (residues 339–452) (Fig. 2d). The β11 strand in part I of the dimer–dimer interface is disordered in the dSelAs.

Catalytic site of dimeric SelA

The catalytic site is located at the subunit interface, involving the core domains and the N-linker, within the intimate dimer unit of SelA. PLP is covalently bound to Lys285, as a Schiff base. Surprisingly, the catalytic site structures of dSelA-FL and dSelA-ΔN differ distinctly from that of the SelA decamer (Fig. 3a–c). The dimeric SelAs lack a SelA-specific β-sheet (β6•β7), and α7 has a distinct orientation. These different catalytic site conformations of the dimeric mutants resemble those of other fold-type-I PLP enzymes (Fig. 3b, c, and e–h). The position of

PLP in the dSelA-ΔN catalytic site is the same as that in the SelA decamer, while dSelA-FL lacked PLP in its catalytic site. PLP may have been removed during the Lys methylation of dSelA-FL, whereas the decameric SelA-FL and SelA-ΔN retained PLP during the methylation [7]. This indicated that the dependentamerization increased the accessibility of Lys285, which probably resulted in the replacement of PLP by a methyl group, although the methyl group was not visible in the structure due to the high mobility of the Lys285 side chain.

The thiosulfate-binding sites also differ from those of the decameric SelA-ΔN (Fig. 3a–c). The decameric SelA-ΔN binds three thiosulfate ions (TS1–TS3) in each catalytic site. TS1 may mimic the substrate selenophosphate, and TS2 and TS3 may mimic the phosphate groups of the nucleotides A76 and C75 of the $tRNA^{Sec}$ CCA terminus [7]. In contrast, dSelA-ΔN binds two thiosulfate ions, TS4 and TS5. TS4 may correspond to TS1, but TS5 does not correspond to any of TS1–TS3. TS1 interacts with $Arg86^{A}$ (subunit A residue) and $Arg312^{B}$ and $Arg315^{B}$ (subunit B residues), whereas TS4 interacts with $Ser172^{A}$, $Arg174^{A}$, $Arg116^{B}$, and $Arg315^{B}$ (Fig. 3d). The distance between TS1 and TS4 is about 3.5 Å. TS5 interacts with $Arg312^{B}$ and $Arg315^{B}$. dSelA-FL also has two thiosulfate ions, TS5 and TS6. TS5 is the same as that in dSelA-ΔN, whereas TS6 occupies the position of the PLP phosphate group. The difference between the thiosulfate-binding sites of dSelA-ΔN and dSelA-FL may be caused by the lack of PLP in the catalytic sites of dSelA-FL.

In decameric SelA, the β6•β7 sheet is stabilized by the pentamerizing interactions. The main chain NH and carbonyl moieties of $Glu168^{A}$ in β6 interact with $Asn193^{J}$, and the $Arg174^{A}$ side chain forms a salt bridge with $Asp199^{J}$ (Fig. 3a). Since $Arg174^{A}$ also participates in α7, the α7 orientation is dependent on the $Arg174^{A}$ position, which is fixed by the $Arg174^{A}$•$Asp199^{J}$ salt bridge. Although the β6•β7 sheet has no polar interactions with the thiosulfate ions, $Gly170^{A}$ in the β6–β7 loop is close to TS1 and forms a van der Waals interaction (Fig. 3a). Therefore, the β6•β7 sheet contributes to TS1 binding and is important for catalysis.

These results indicated that the formation of the catalytic site structure is dependent on the pentamerization of intimate dimers and that the dimeric mutant cannot properly bind its substrates. The activity loss by the mutations introduced to the pentamerization interfaces (Table 1) should result from both the prevention of decamer-dependent $tRNA^{Sec}$ binding and the disruption of the catalytic core structure.

How does SelA eliminate the hydroxyl group from the Ser moiety?

In general, proper binding and hydroxyl-group protonation of the substrate are essential for an enzyme to eliminate a hydroxyl group. SelA has a putative binding pocket for the A76 adenine ring (Fig. 4a) [7] and can therefore accommodate the Ser moiety of Ser-$tRNA^{Sec}$. This binding pocket is critically important because Ser-$tRNA^{Sec}$ lacks the α-carboxyl group, which is used for the substrate–enzyme interaction in all of the fold-type-I superfamily PLP-dependent enzymes working on α-amino acids [10].

To examine the mechanism of hydroxyl-group protonation, we compared SelA with other PLP-dependent enzymes. SelA is the only fold-type-I enzyme that eliminates the hydroxyl group from the substrate amino acid (or amino acid moiety). Therefore, we compared SelA with cystathionine β-synthase (CBS), a fold-type-II PLP-dependent enzyme that catalyzes a β replacement reaction. CBS eliminates the hydroxyl group from serine to generate 2-aminoacrylate and then adds homocysteine to synthesize cystathionine (Supplementary Fig. 1a). The β elimination step is the same as that in SelA catalysis (Fig. 1). A crystallographic study revealed that Tyr227 of CBS is responsible for the protonation of the serine hydroxyl group [14]. Interestingly, cysteine synthase (CysS), the close homolog of CBS, lacks the corresponding Tyr residue [15]. CysS catalyzes the β replacement reaction that eliminates an acetyl group from *O*-acetylserine, and it adds hydrogen sulfide to generate cysteine (Supplementary Fig. 1b). In this reaction, the leaving group is acetate, and thus, hydroxyl-group protonation is unnecessary.

On the other hand, SelA lacks residues such as Tyr, His, and Cys that could serve as proton donors in the vicinity of the Ser-moiety-binding site, except for Lys285, which forms a Schiff base with PLP in the waiting state. Some enzymes in the sugar aminotransferase subfamily catalyze the elimination of the α-hydrogen and the β-hydroxyl group. Here, the α position indicates the position of the amino group conjugated with PLP during catalysis. The enzymes GDP-6-deoxy-α-D-*lyxo*-hexopyranos-4-ulose dehydratase (ColD) and CDP-6-deoxy-α-D-*xylo*-hexopyranos-4-ulose dehydratase (E_1) employ a His residue, which is conserved at the position of the PLP-coordinating Lys285 of SelA, to catalyze the α,β elimination step (Supplementary Fig. 1c and d) [16,17]. In contrast, 5-amino-3-hydroxybenzoate (AHBA) synthase, another enzyme that eliminates the α-hydrogen and the β-hydroxyl group (Supplementary Fig. 1e), contains a conserved Lys residue, which is considered to protonate the β-hydroxyl group [18]. Here, the generation of a benzene ring in the product is likely to promote the α,β elimination reaction.

These findings suggested that Lys285 in SelA can act as proton donor for the β-hydroxyl group (Fig. 4b). As enzymes such as ColD and E_1 utilize His, instead of Lys, to strengthen the protonation activity and AHBA generates a benzene ring to promote the

Fig. 6. Structure-based phylogenetic tree of the fold-type-I PLP-dependent enzymes. SelA and the crystal structures of the fold-type-I PLP enzymes, deposited in the Protein Data Bank, were analyzed. The enzyme names are colored based on their catalysis type: the enzymes that catalyze aminotransfer (AT), α-carboxyl group replacement, α-hydrogen replacement, reverse aldol reaction, α,β elimination, β replacement (type 1), β replacement (type 2), α,γ elimination, and γ replacement are colored dark blue, blue, sky blue, blue-violet, magenta, red, orange, spring green, and green, respectively. The enzymes with unknown functions are colored gray. The structure-based phylogenetic analysis revealed that SelA, SepSecS, and SepCysS [20] belong to distinct taxa of the fold-type-I PLP-dependent enzymes. SelA is likely to form an independent group related to the cystathionine γ-synthase (CGS) family. SepCysS is close to the cysteine desulfurase and kynureninase families, while SepSecS also forms another independent group close to the sugar aminotransferase (AT) family.

protonation and elimination of the β-hydroxyl group, an additional auxiliary mechanism to support protonation and β-hydroxyl elimination might be plausible for SelA as well. Such a mechanism would involve the Arg86 residue (Fig. 4a and b). Our *in vivo* mutational assay revealed that Arg86 is mandatory for activity [7]. Arg86 is located in the vicinity of Lys285 (Fig. 4a), and the positive charge of Arg86 may reinforce the protonation activity of Lys285. Arg86 is located in the N-linker between the N and core domains. The β-strand β1 in the N-linker forms a β-sheet with β18 from the C-terminal domain (Fig. 4c). Although the corresponding β-sheet is present in many fold-type-I PLP-dependent enzymes, the C-terminal domain

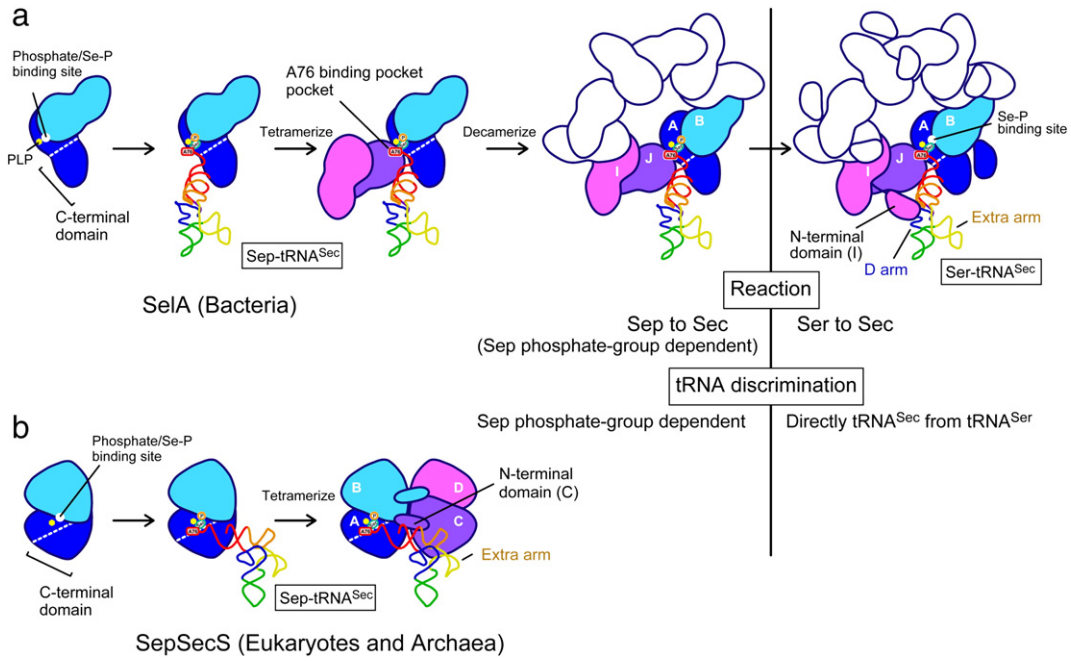

Fig. 7. Possible steps of SelA (a) and SepSecS (b) evolution. The dimeric SelA ancestor accommodated the $tRNA^{Sec}$ acceptor arm within the cleft between the core and C-terminal domains. The ancestor interacted with the substrate $Sep\text{-}tRNA^{Sec}$ by binding its Sep phosphate group at the selenophosphate (Se-P)-binding site. Therefore, the Sep-to-Sec reaction and the tRNA discrimination were dependent on the Sep phosphate group. Tetramerization created the A76-binding pocket, and decamerization stabilized the interactions among intimate dimers. Finally, the acquired N-terminal domain discriminated $tRNA^{Sec}$ from $tRNA^{Ser}$, by interacting with the unique D arm of $tRNA^{Sec}$. The A76-binding pocket and the $tRNA^{Sec}$ discrimination enabled Ser-to-Sec conversion, and thus, SelA became independent of the Sep phosphate group. On the other hand, the dimeric SepSecS interacted with the extra arm side of the $tRNA^{Sec}$ acceptor arm, since it lacks the cleft between the core and C-terminal domains. Tetramerization stabilized the $tRNA^{Sec}$ binding by interacting with its T and extra arms, without recognizing the unique D arm structure. Therefore, SepSecS is unable to become independent of the Sep phosphate group of $Sep\text{-}tRNA^{Sec}$.

orientation in SelA differs from those of the other homologs (Fig. 5). The unique C-terminal domain orientation in SelA results in the specific positioning of the N-linker that allows participation in the catalytic site. This structural feature is the reason why the N-linker can provide Arg86 in the vicinity of Lys285. Here again, the characteristic tertiary and quaternary structures of SelA are essential for its unique catalytic activity to eliminate the hydroxyl group.

SepSecS also possesses an Arg residue (Arg75 in human SepSecS) that occupies the space corresponding to SelA Arg86 [9]. However, Arg75 is located in the core domain of SepSecS and is not an alignment-based counterpart of SelA Arg86, which is in the N-linker. In fact, Arg75 forms an intersubunit interaction with Lys-bound PLP; that is, $Arg75^{B}$ interacts with $PLP\text{-}Lys284^{A}$ (Fig. 3e). In contrast, the Arg86 and PLP-Lys285 interaction is an intrasubunit one (Figs. 3a and 4a). Moreover, the PLP-ligated Lys284 in SepSecS cannot protonate the β-hydroxyl group of the Ser moiety; SepSecS cannot bind $Ser\text{-}tRNA^{Sec}$ because the phosphate group of the Sep moiety is essential for the substrate $Sep\text{-}tRNA^{Sec}$ binding.

Why did two different pathways for Sec formation evolve?

Considerable conservation of the translation machinery components exists among the three domains of life. However, the pathways of aminoacyl-tRNA formation evolved much more independently. For instance, the synthesis of Asn-tRNA or Gln-tRNA involves tRNA-dependent and tRNA-independent amino acid biosynthesis routes [19]. In the case of Sec, nature also designed distinct routes based on the different enzyme structures operating in Bacteria *versus* Archaea/Eukaryotes. Our phylogenetic analysis (Fig. 6) revealed that SelA is related to the cystathionine γ-synthase (CGS) family members catalyzing the β elimination of cysteine derivatives or the γ elimination and γ replacement of homocysteine products. Thus, the ancestor of SelA may have been an enzyme involved in sulfur metabolism. The protein

Table 2. Data collection and refinement statistics.

	dSelA-FL^{4KA} (SeMet)	dSelA-ΔN (SeMet)
Lys methylation	+	–
Data collection		
Beam line	SPring-8 BL41XU	SPring-8 BL41XU
Wavelength (Å)	0.97915	0.97915
Space group	*I*422	$P2_1$
Cell parameters		
a (Å)	144.1	59.2
b (Å)	144.1	81.3
c (Å)	273.4	95.5
β (°)		92.2
Resolution (Å)	50.0–3.35 (3.47–3.35)[a]	50.0–2.40 (2.49–2.40)[a]
Unique reflections	21,096 (2066)[a]	35,457 (3520)[a]
Completeness (%)	99.7 (100.0)[a]	99.6 (100.0)[a]
Redundancy	6.0 (6.1) [a]	3.8 (3.8)[a]
R_{sym}[b]	0.102 (0.712)[a]	0.082 (0.561)[a]
$I/\sigma(I)$	17.2 (2.75)[a]	15.9 (2.40)[a]
Structure refinement		
Working-set reflections	19,970	33,593
Test-set reflections	1062	1770
Resolution (Å)	50.0–3.35	50.0–2.40
Number of SelA subunits	2 (one dimer)	2 (one dimer)
Number of protein atoms	7035	6018
Number of PLP	0	2
Number of ions	4 (thiosulfate)	5 (thiosulfate)
Number of solvent molecules	0	153
R_{work}/R_{free}[c]	0.194/0.250	0.180/0.230
Average B-factor (Å^2)		
Overall	144.3	64.4
Protein	144.2	64.6
PLPs	—	49.8
Ion	162.4	79.0
Solvent	—	56.7
RMSD bond lengths (Å)	0.009	0.008
RMSD bond angles (°)	1.27	1.12

[a] The statistics in the highest-resolution shell are given in parentheses.
[b] $R_{sym} = \sum_{hkl}\sum_i[|I_i(hkl) - \langle I(hkl)\rangle|]/\sum_{hkl}\sum_i[I_i(hkl)]$, where $I_i(hkl)$ is the intensity of the *i*th measurement of *hkl* and $\langle I(hkl)\rangle$ is the average value of $I_i(hkl)$ for all *i*th measurements.
[c] $R_{work,free} = \sum_{hkl}(||F_o| - k|F_c||)/\sum_{hkl}(|F_o|)$, where R_{work} and R_{free} are calculated using the working-set and test-set reflections (5% of the total reflections), respectively.

closest to SelA in the phylogenetic tree is the archaeal MJ0158, a homodimeric protein of unknown function that does not interact with tRNA^{Sec} (Fig. 6) [13]. Interestingly, the orientation of the C-terminal domain of MJ0158 is similar to that of the SelA C-terminal domain (Fig. 5d and h), suggesting that the change in the domain orientation occurred before SelA acquired its function. Although the N-linker of MJ0158 occupies the similar space to that of SelA, MJ0158 has a Ser residue at the corresponding position of SelA Arg86, which may reflect its functional difference from SelA.

Since the binding of the A76-Ser moiety of Ser-tRNA is impossible without the decameric assembly (the putative A76-binding site is formed at the dimer–dimer interface) [7], it is plausible that a dimeric SelA ancestor depended on the phosphate group and simply converted Sep to Sec without tRNA^{Sec} discrimination, as in the case of SepSecS (Fig. 7). In fact, the extant SelA can produce Sec-tRNA^{Sec} from Ser-tRNA^{Sec} and from Sep-tRNA^{Sec} [5], confirming that the Sec synthesis by SelA does not rely on the phosphate group of the substrate aminoacyl moiety. Like SepSecS, the SelA ancestor may have used its selenophosphate-binding site to bind the Sep phosphate moiety in order to facilitate the elimination of the phosphate group from Sep. In this case, either PSTK or an enzyme with a similar function must have existed for the phosphorylation of Ser and the discrimination of tRNA^{Sec} from tRNA^{Ser}. Alternatively, the ability of SepSecS to convert Ser to Sec was lost when PSTK evolved for more efficient Sec production.

Evolving decamerization

In a subsequent evolutionary step, the collaboration of the two SelA dimers could have occurred to

generate the A76-binding pocket at the dimer–dimer interface, thereby improving the efficiency and specificity of substrate binding. Nonetheless, in such a tetramer, only two of the four catalytic sites would have been functional (the "half-of-the-sites" stage). The relative orientations between the dimers could then be stabilized by acquiring decameric ring closure involving five dimers. Simultaneously, the full usage of all 10 catalytic sites was achieved (Fig. 7a). Interestingly, the non-productive catalytic site conformation of the dimeric mutant dSelA-ΔN resembles those of the other fold-type-I members (Fig. 3b, c, and e–h) and therefore appears to be more primeval. The loop region before α7 interacts with PLP in dSelA-ΔN (Fig. 3b and c), while it forms a β-sheet (β6•β7) in the SelA decamer (Fig. 3a). Hence, the catalytic site may have evolved by taking advantage of the decameric quaternary structure. The N-terminal domain was then acquired to increase its affinity for $tRNA^{Sec}$ and was further utilized for the discrimination of $tRNA^{Sec}$ from $tRNA^{Ser}$.

Conclusion

The natural decameric arrangement of five SelA dimers allows the formation of 10 fully occupied and catalytically functional active sites. Since SelA decamerization is driven by dimer–dimer interactions, disruptive mutations at the interaction interfaces solely yield SelA dimers. In striking contrast to decameric SelA, these dimers are catalytically deficient and exhibit a distinctly distorted active-site formation that prevents productive $tRNA^{Sec}$ coordination. In fact, the dimeric SelA conformationally resembles similar related PLP enzymes, such as the tetrameric SepSecS. The evolution of the SelA decamer may have been driven by enhanced catalytic efficiency obtained from two sources: First, the decamer allows for an active-site conformation that is optimal for direct, tRNA-dependent Ser-to-Sec conversion. Second, the 10-subunit architecture of SelA generates an N-terminal domain with the ability to discriminate $tRNA^{Sec}$.

Materials and Methods

Protein preparation

The genes encoding the full-length and ΔN SelA genes from *A. aeolicus* were cloned into the vectors pET25b and pET22b (Novagen), respectively. The full-length SelA used for crystallization was a quadruple mutant, with the non-conserved Lys residues in the loop regions of the N-terminal domain replaced by Ala residues, Lys19Ala-Lys21Ala-Lys46Ala-Lys48Ala (SelA-FL^{4KA}). The dimerizing quadruple mutation, Tyr220Pro-Asp199Arg-Thr191Tyr-Thr192Tyr, was introduced into SelA-FL^{4KA} and SelA-ΔN by QuikChange site-directed mutagenesis (Stratagene). The *E. coli* strain Rosetta 2(DE3) (Stratagene) was transformed with the expression plasmids, and the native and selenomethionine (SeMet)-substituted proteins were overexpressed and purified as previously described [21]. In order to improve the crystallization efficiency, we methylated the lysine residues of dSelA-FL^{4KA} with formaldehyde and a dimethylamine–borane complex, as previously described [22]. Prior to methylation, the protein was diluted with 20 mM Hepes–NaOH buffer (pH 7.5), containing 0.8 M NaCl and 10 mM 2-mercaptoethanol.

Crystallization and X-ray diffraction data collection

The SelA proteins were crystallized at 20 °C by the sitting-drop vapor diffusion method, by mixing 0.75 μl of the sample with 0.75 μl of reservoir solutions. Prior to crystallization, dSelA-FL^{4KA} (SeMet substitution, Lys methylation) and dSelA-ΔN (SeMet substitution, without methylation) were dialyzed against 20 mM Tris–HCl buffer (pH 7.5), containing 200 mM NaCl and 10 mM 2-mercaptoethanol, and were concentrated to 9.6 and 7.8 mg/ml, respectively.

Crystal Screen 2, Natrix (Hampton Research), Wizard I, and Wizard II (Emerald Bio-Science) screening kits were used for the initial screening of the crystallization conditions. The optimized reservoir solutions were 100 mM trisodium citrate–HCl buffer (pH 5.6), containing 580–590 mM trisodium citrate, 100 mM L-serine, and 100 mM $Na_2S_2O_3$ for dSelA-FL^{4KA}, as well as 100 mM sodium 4-morpholineethanesulfonate HCl buffer (pH 6.5), containing 2.5% polyethylene glycol 4000, 150 mM $Na_2S_2O_3$, and 70 mM $NaNO_3$ for dSelA-ΔN.

The crystals thus obtained were transferred into cryo-protective solutions composed of 100 mM trisodium citrate–HCl buffer (pH 5.6), containing 1.3 M trisodium citrate, 75 mM L-serine, and 75 mM $Na_2S_2O_3$ for dSelA-FL^{4KA}, as well as 100 mM sodium 4-morpholineethanesulfonate HCl buffer (pH 6.5), containing 30% dimethyl sulfoxide, 10% polyethylene glycol 4000, 50 mM $Na_2S_2O_3$, and 70 mM $NaNO_3$ for dSelA-ΔN, and were flash-cooled in a cryo-N_2 stream. X-ray diffraction data were collected at 90 K by using synchrotron radiation at the BL41XU of SPring-8 (Harima, Japan). The data were processed with the HKL2000 program [23]. The statistics of the diffraction data collection are listed in Table 2.

Structure determination and refinement

The structures of the dimeric SelAs, dSelA-FL^{4KA} and dSelA-ΔN, were solved by the molecular replacement method, using the Phaser program [24]. The search model was the SelA-ΔN structure. The Coot program [25] was used for manual fitting of the models to the electron density map. The structures were refined against the diffraction data by using the CNS [26] and PHENIX [27] programs, with iterative cycles of positional and temperature factor refinements (Table 2).

Production and purification of *E. coli* SelA variants

Mutations were introduced by site-directed mutagenesis (QuikChange®; Agilent) to *E. coli* K12 *selA,* from the ASKA *E. coli* K12 ORF library (GFP-minus), cloned in the pC24N vector [28]. *E. coli* BL21 cells were transformed with the expression plasmids. For protein overproduction, the cells

were grown at 25 °C in LB selective medium, supplemented with 50 μM isopropyl β-D-1-thiogalactopyranoside. Cells sedimented from overnight cultures were resuspended in lysis buffer (50 mM KH_2PO_4, pH 8, 300 mM NaCl, 15% glycerol, 10 mM imidazole) and disrupted by sonication. After centrifugation (50,000*g*, 45 min, 4 °C), the clarified lysates were subjected to immobilized metal affinity chromatography, using Ni-NTA affinity resin (Qiagen) on gravity-flow columns. The immobilized 6× His-SelA fusion proteins were washed with lysis buffer supplemented with 40 mM imidazole, and SelA was eluted with 240 mM imidazole in lysis buffer. The excess imidazole was removed by dialysis (50 mM Tris–HCl, pH 7.5, 300 mM NaCl, 15% glycerol), and the purified SelA variants were analyzed by SDS-PAGE and stored at −80 °C. The amounts of protein-bound PLP in the SelA variants were determined by UV/vis spectroscopy at 420 nm and in comparison to a PLP standard curve (0–2 mM).

E. coli SelA *in vivo* activity assays

For *in vivo* SelA assays, a marker-less *E. coli* selA deletion strain was used. The initial *selA* deletion strain JS1 was constructed by the replacement of the *selA* gene with a kanamycin cassette in *E. coli* strain BW25113, as previously described [29], and the genomic insertion of T7 polymerase by P1 transduction [4]. The kanamycin resistance marker of *E. coli* strain JS1 was then excised by FLP recombinase-mediated homologous recombination between the FRT sites flanking the kanamycin resistance cassette, upon transformation of the JS1 strain with the plasmid pCP20 [30], resulting in the marker-less *E. coli* Δ*selA* strain JS2. *E. coli* Δ*selA* was then transformed with the plasmids encoding the *E. coli* SelA variants and grown on LB selective medium. Overnight cultures of these clones were plated on selective LB agar plates supplemented with 10 μM isopropyl β-D-1-thiogalactopyranoside, 1 μM Na_2MoO_4, 1 μM Na_2SeO_3, and 50 mM sodium formate, as described previously [4], and grown anaerobically at 37 °C overnight. For the oxygen-sensitive benzyl viologen assay, the plates were transferred to an anaerobic chamber (90% N_2, 5% H_2, 5% CO_2) and overlaid with top agar containing 1 mg/ml benzyl viologen, 250 mM sodium formate, and 25 mM KH_2PO_4/K_2HPO_4 (pH 7.0). Wild-type SelA served as a positive control. The benzyl viologen assay allows the colorimetric monitoring of SelA activity by the formation of purple-colored reduced benzyl viologen. Benzyl viologen reduction is catalyzed by FDH_H, which requires Sec insertion for catalytic activity. The Sec formation, finally, is dependent on the SelA activity.

Structure-based phylogenetic tree

The STAMP program [31] in the MultiSeq module of VMD [32] was used to superpose and calculate the structural similarity, Q_H, among the coordinates of SelA-ΔN and the other fold-type-I PLP-dependent enzymes obtained from the Protein Data Bank. The enzymes with >50% amino acid sequence identity were removed, and thus, the core domains of 187 coordinates, including the coordinates of both chains A and B of the heterodimeric glycine decarboxylase (PDB ID: 1WYT), were superposed. The other 185 enzymes were homooligomeric ones. The structural similarity Q_H was calculated [33], and the neighbor-joining tree, based on the Q_H values, was drawn using the SplitsTree program [34].

Accession numbers

The coordinates and structure factors have been deposited in the Protein Data Bank (PDB IDs: 3WCN and 3WCO).

Supplementary data to this article can be found online at http://dx.doi.org/10.1016/j.jmb.2014.01.003.

Acknowledgments

We thank the staff members of SPring-8 BL41XU and the Photon Factory beam lines for assistance with our data collection. We thank T. Imada, K. Ake, and T. Nakayama for assistance with the manuscript preparation and P. O'Donoghue and M. Simonovic (University of Illinois, Chicago) for critical discussions. We are grateful to the National BioResource Project in Japan for providing the ASKA *E. coli* K12 ORF library. Y.I. was supported by Research Fellowships from the Japan Society for the Promotion of Science. M.J.B. holds a Feodor Lynen Postdoctoral Fellowship of the Alexander von Humboldt Foundation (Bonn, Germany). This work was supported in part by Japan Society for the Promotion of Science Grants-in-Aid for Scientific Research (A) to S.Y. and (C) to S.S. This work was also supported in part by the Targeted Proteins Research Program, and the Platform for Drug Discovery, Informatics, and Structural Life Science from the Ministry of Education, Culture, Sports, Science, and Technology (to S.Y.). D.S. gratefully acknowledges support from the Division of Chemical Sciences, Geosciences, and Biosciences, Office of Basic Energy Sciences of the U.S. Department of Energy (DE-FG02-98ER20311; for funding the genetic experiments), from the National Institute of General Medical Sciences (GM22854), and from the Defense Advanced Research Projects Agency (contracts N66001-12-C-4020 and N66001-12-C-4211).

Received 8 November 2013;
Received in revised form 9 January 2014;
Accepted 12 January 2014
Available online 20 January 2014

Keywords:
fold-type-I PLP-dependent enzyme;
selenium metabolism;
$tRNA^{Sec}$;
pentamer of dimers;
21st amino acid

Y.I. and M.J.B. contributed equally to this work.

Abbreviations used:
AHBA, 5-amino-3-hydroxybenzoate; CBS, cystathionine β-synthase; CysS, cysteine synthase; PLP, pyridoxal 5′-phosphate; PSTK, *O*-phosphoseryl-tRNA^{Sec} kinase; SeMet, selenomethionine.

References

[1] Böck A, Forchhammer K, Heider J, Leinfelder W, Sawers G, Veprek B, et al. Selenocysteine: the 21st amino acid. Mol Microbiol 1991;5:515–20.

[2] Ehrenreich A, Forchhammer K, Tormay P, Veprek B, Böck A. Selenoprotein synthesis in *E. coli*. Purification and characterisation of the enzyme catalysing selenium activation. Eur J Biochem 1992;206:767–73.

[3] Carlson BA, Xu XM, Kryukov GV, Rao M, Berry MJ, Gladyshev VN, et al. Identification and characterization of phosphoseryl-tRNA$^{[Ser]Sec}$ kinase. Proc Natl Acad Sci U S A 2004;101:12848–53.

[4] Yuan J, Palioura S, Salazar JC, Su D, O'Donoghue P, Hohn MJ, et al. RNA-dependent conversion of phosphoserine forms selenocysteine in eukaryotes and archaea. Proc Natl Acad Sci U S A 2006;103:18923–7.

[5] Xu XM, Carlson BA, Mix H, Zhang Y, Saira K, Glass RS, et al. Biosynthesis of selenocysteine on its tRNA in eukaryotes. PLoS Biol 2007;5:e4.

[6] Forchhammer K, Böck A. Selenocysteine synthase from *Escherichia coli*. Analysis of the reaction sequence. J Biol Chem 1991;266:6324–8.

[7] Itoh Y, Bröcker MJ, Sekine S, Hammond G, Suetsugu S, Söll D, et al. Decameric SelA•tRNA^{Sec} ring structure reveals mechanism of bacterial selenocysteine formation. Science 2013;340:75–8.

[8] Clausen T, Huber R, Laber B, Pohlenz HD, Messerschmidt A. Crystal structure of the pyridoxal-5′-phosphate dependent cystathionine beta-lyase from *Escherichia coli* at 1.83 Å. J Mol Biol 1996;262:202–24.

[9] Palioura S, Sherrer RL, Steitz TA, Söll D, Simonovic M. The human SepSecS-tRNA^{Sec} complex reveals the mechanism of selenocysteine formation. Science 2009;325:321–5.

[10] Eliot AC, Kirsch JF. Pyridoxal phosphate enzymes: mechanistic, structural, and evolutionary considerations. Annu Rev Biochem 2004;73:383–415.

[11] Araiso Y, Sherrer RL, Ishitani R, Ho JM, Söll D, Nureki O. Structure of a tRNA-dependent kinase essential for selenocysteine decoding. Proc Natl Acad Sci U S A 2009;106:16215–20.

[12] Fukunaga R, Yokoyama S. Structural insights into the second step of RNA-dependent cysteine biosynthesis in archaea: crystal structure of Sep-tRNA:Cys-tRNA synthase from *Archaeoglobus fulgidus*. J Mol Biol 2007;370:128–41.

[13] Kaiser JT, Gromadski K, Rother M, Engelhardt H, Rodnina MV, Wahl MC. Structural and functional investigation of a putative archaeal selenocysteine synthase. Biochemistry 2005;44:13315–27.

[14] Koutmos M, Kabil O, Smith JL, Banerjee R. Structural basis for substrate activation and regulation by cystathionine beta-synthase (CBS) domains in cystathionine β-synthase. Proc Natl Acad Sci U S A 2010;107:20958–63.

[15] Burkhard P, Tai CH, Ristroph CM, Cook PF, Jansonius JN. Ligand binding induces a large conformational change in *O*-acetylserine sulfhydrylase from *Salmonella typhimurium*. J Mol Biol 1999;291:941–53.

[16] Cook PD, Thoden JB, Holden HM. The structure of GDP-4-keto-6-deoxy-D-mannose-3-dehydratase: a unique coenzyme B6-dependent enzyme. Protein Sci 2006;15:2093–106.

[17] Chen XM, Ploux O, Liu HW. Biosynthesis of 3,6-dideoxyhexoses: *in vivo* and *in vitro* evidence for protein–protein interaction between CDP-6-deoxy-L-threo-D-glycero-4-hexulose 3-dehydrase (E1) and its reductase (E3). Biochemistry 1996;35:16412–20.

[18] Eads JC, Beeby M, Scapin G, Yu TW, Floss HG. Crystal structure of 3-amino-5-hydroxybenzoic acid (AHBA) synthase. Biochemistry 1999;38:9840–9.

[19] Ambrogelly A, Palioura S, Soll D. Natural expansion of the genetic code. Nat Chem Biol 2007;3:29–35.

[20] Sauerwald A, Zhu W, Major TA, Roy H, Palioura S, Jahn D, et al. RNA-dependent cysteine biosynthesis in archaea. Science 2005;307:1969–72.

[21] Itoh Y, Sekine S, Yokoyama S. Crystallization and preliminary X-ray crystallographic analysis of *Aquifex aeolicus* SelA, a bacterial selenocysteine synthase. Acta Crystallogr Sect F Struct Biol Cryst Commun 2012;68:1128–33.

[22] Walter TS, Meier C, Assenberg R, Au KF, Ren J, Verma A, et al. Lysine methylation as a routine rescue strategy for protein crystallization. Structure 2006;14:1617–22.

[23] Otwinowski Z, Minor W. Processing of X-ray diffraction data collected in oscillation mode. Methods Enzymol 1997;276:307–26.

[24] McCoy AJ, Grosse-Kunstleve RW, Adams PD, Winn MD, Storoni LC, Read RJ. Phaser crystallographic software. J Appl Crystallogr 2007;40:658–74.

[25] Emsley P, Cowtan K. Coot: model-building tools for molecular graphics. Acta Crystallogr Sect D Biol Crystallogr 2004;60:2126–32.

[26] Adams PD, Pannu NS, Read RJ, Brunger AT. Cross-validated maximum likelihood enhances crystallographic simulated annealing refinement. Proc Natl Acad Sci U S A 1997;94:5018–23.

[27] Adams PD, Afonine PV, Bunkóczi G, Chen VB, Davis IW, Echols N, et al. PHENIX: a comprehensive Python-based system for macromolecular structure solution. Acta Crystallogr Sect D Biol Crystallogr 2010;66:213–21.

[28] Kitagawa M, Ara T, Arifuzzaman M, Ioka-Nakamichi T, Inamoto E, Toyonaga H, et al. Complete set of ORF clones of *Escherichia coli* ASKA library (a complete set of *E. coli* K-12 ORF archive): unique resources for biological research. DNA Res 2005;12:291–9.

[29] Datsenko KA, Wanner BL. One-step inactivation of chromosomal genes in *Escherichia coli* K-12 using PCR products. Proc Natl Acad Sci U S A 2000;97:6640–5.

[30] Yuan J, Hohn MJ, Sherrer RL, Palioura S, Su D, Söll D. A tRNA-dependent cysteine biosynthesis enzyme recognizes the selenocysteine-specific tRNA in *Escherichia coli*. FEBS Lett 2010;584:2857–61.

[31] Roberts E, Eargle J, Wright D, Luthey-Schulten Z. MultiSeq: unifying sequence and structure data for evolutionary analysis. BMC Bioinformatics 2006;7:382.

[32] Humphrey W, Dalke A, Schulten K. VMD: visual molecular dynamics. J Mol Graphics 1996;14:27–8.

[33] O'Donoghue P, Luthey-Schulten Z. Evolutionary profiles derived from the QR factorization of multiple structural alignments gives an economy of information. J Mol Biol 2005;346:875–94.

[34] Huson DH, Bryant D. Application of phylogenetic networks in evolutionary studies. Mol Biol Evol 2006;23:254–67.